



Titre: A comparative study of fibre Bragg grating for spatially and temporally resolved gas temperature measurements in cold atmospheric pressure plasma jets
Title:

Auteurs: Jean-Baptiste Billeau, Jyothis Thomas, Raman Kashyap, Derek Rosenzweig, & Stephan Reuter
Authors:

Date: 2024

Type: Article de revue / Article

Référence: Billeau, J.-B., Thomas, J., Kashyap, R., Rosenzweig, D., & Reuter, S. (2024). A comparative study of fibre Bragg grating for spatially and temporally resolved gas temperature measurements in cold atmospheric pressure plasma jets. Plasma Sources Science and Technology, 33(10), 105004 (8 pages).
Citation: <https://doi.org/10.1088/1361-6595/ad7be9>

 **Document en libre accès dans PolyPublie**
Open Access document in PolyPublie

URL de PolyPublie: <https://publications.polymtl.ca/59467/>
PolyPublie URL:

Version: Version officielle de l'éditeur / Published version
Révisé par les pairs / Refereed

Conditions d'utilisation: CC BY
Terms of Use:

 **Document publié chez l'éditeur officiel**
Document issued by the official publisher

Titre de la revue: Plasma Sources Science and Technology (vol. 33, no. 10)
Journal Title:

Maison d'édition: IOP Publishing
Publisher:

URL officiel: <https://doi.org/10.1088/1361-6595/ad7be9>
Official URL:

Mention légale: Original content from this work may be used under the terms of the Creative Commons Attribution 4.0 licence (<https://creativecommons.org/licenses/by/4.0/>). Any further distribution of this work must maintain attribution to the author(s) and the title of the work, journal citation and DOI.
Legal notice:

PAPER • OPEN ACCESS

A comparative study of fibre Bragg grating for spatially and temporally resolved gas temperature measurements in cold atmospheric pressure plasma jets

To cite this article: Jean-Baptiste Billeau *et al* 2024 *Plasma Sources Sci. Technol.* **33** 105004

View the [article online](#) for updates and enhancements.

You may also like

- [Numerical investigation of vacuum ultra-violet emission in Ar/O₂ inductively coupled plasmas](#)

Michel Osca Engelbrecht, Jonathan Jenderny, Henrik Hylla *et al.*

- [Collision integrals of electronically excited atoms in air plasmas. I. N–N and O–O interactions](#)

Wensheng Zhao, Qizhen Hong, Chao Yang *et al.*

- [Validation of the thermo-chemical approach to modelling of CO₂ conversion in sub-atmospheric pressure microwave gas discharges](#)

Vladislav Kotov, Christian Kiefer and Ante Hecimovic



HIDEN ANALYTICAL

Analysis Solutions for your Plasma Research

For Surface Science

- ▶ Surface Analysis
- ▶ SIMS
- ▶ 3D depth Profiling
- ▶ Nanometre depth resolution

■ Compact SIMS

■ SIMS Workstation

■ Auto SIMS

For Plasma Diagnostics

- ▶ Plasma characterisation
- ▶ Customised systems to suit plasma Configuration
- ▶ Mass and energy analysis of plasma ions
- ▶ Characterisation of neutrals and radicals

■ ESPion

■ HPR-60 MBMS



■ EQP Series

Click to view our product catalogue

■ Knowledge ■ Experience ■ Expertise

Contact Hiden Analytical for further details:
W www.HidenAnalytical.com
E info@hiden.co.uk

A comparative study of fibre Bragg grating for spatially and temporally resolved gas temperature measurements in cold atmospheric pressure plasma jets

Jean-Baptiste Billeau^{1,*} , Jyothis Thomas¹, Raman Kashyap¹, Derek Rosenzweig^{2,3} and Stephan Reuter^{1,*} 

¹ Department of Engineering Physics, Polytechnique Montreal, Montreal QC H3T 1J4, Canada

² Department of Surgery, McGill University, Montreal QC H3G 1A4, Canada

³ Injury, Repair and Recovery Program, Research Institute of McGill University Health Centre, Montreal QC H3H 2R9, Canada

E-mail: jean-baptiste.billeau@polymtl.ca and stephan.reuter@polymtl.ca

Received 7 December 2023, revised 9 May 2024

Accepted for publication 17 September 2024

Published 7 October 2024



CrossMark

Abstract

Cold atmospheric pressure plasma jets (CAP-Jet) are successfully used in medical therapy for healing of chronic wounds and are widely researched in inactivation of pathogens and in assisting in cancer therapy. A crucial parameter for these plasma applications is that CAP-Jets operate at temperatures that are tolerable for biological tissues. While tools characterizing the plasma's gas temperature are well developed, there are only a few methods that work with an agreeable limit of uncertainty, complexity and limited perturbation properties to accurately determine that the studied plasma jet operates at tissue tolerable temperatures at all times. In the current work, time resolved measurements of the gas temperature in the effluent of a CAP-Jet are performed using the innovative technique of a fibre Bragg grating (FBG), in which the temperature dynamics is measured by a shift of the FBGs resonant wavelength through its thermo-optic coefficient. Comparing with other temporal and spatial diagnostic tools such as thermocouple measurement, Schlieren imaging, and optical emission spectroscopy, we demonstrate reliable calorimetric measurements at different plasma duty cycles. The plasma source maintains tissue tolerable temperatures inside the plasma active zone with values below 35 °C at 1 cm distance from the jet nozzle. The calorimetric measurements have revealed that the heat power dissipation in comparison to electric energy of our plasma source is at least 50%.

Keywords: atmospheric pressure plasma, fibre Bragg grating, temperature measurements, schlieren

* Authors to whom any correspondence should be addressed.



Original content from this work may be used under the terms of the [Creative Commons Attribution 4.0 licence](https://creativecommons.org/licenses/by/4.0/). Any further distribution of this work must maintain attribution to the author(s) and the title of the work, journal citation and DOI.

1. Introduction

Over the past two decades, plasma medicine has emerged as an exciting new therapy for wounds healing, and as a successful tool for infection treatment, and is promising for cancer and immunotherapy [1–6]. Cold atmospheric pressure plasma jets (CAP-Jets) have gained much attention for their application potential in medicine, primarily through delivering of a temporally and spatially confined oxy-nitroso stress burst [7]. The complex interaction process of plasma and biological systems generates reactive oxygen and nitrogen species (RONS) that trigger cell death mechanisms and modify cell signalling pathways [8]. By controlling parameters like electric field, gas composition, and energy input, various biological responses can be induced. Particularly for thermally sensitive biological tissues, an exact knowledge of the plasma's gas temperature becomes paramount for controlling RONS production while mitigating any adverse thermal effects [9].

Conventional gas temperature measurements typically are performed with electrical thermocouples [10, 11], by emission and absorption spectroscopy [12–14], by laser-induced fluorescence [15–17], with fluoro-optic probing [18], and with Schlieren imaging [19, 20]. However, these techniques often introduce substantial uncertainties to the overall temperature evaluation or necessitate complex manipulations and analysis. The present work proposes for an electrically non-invasive type of temperature measurement a more approachable measurement of the plasma's gas temperature made for the first time in CAP-Jet with a fibre Bragg grating (FBG). The inherent dielectric property of the FBG renders it resilient to significant potential interferences from high voltage, high frequency and gas composition variations, thereby enhancing measurement accuracy. As an optical method, FBG distinguishes itself from other fibre-based method by its ability to integrate multiple sensors in a single fibre, thus increasing its sensitivity through wavelength-division multiplexing [21]. While temperature measurement by FBG and thermocouple were already proven to be used for long duration in harsher plasma environment [22], the scope of this article is to explore the reliability of the technique in thermally biocompatible conditions. In order to validate the FBG temperature measurements, we compared the measurements to those with a bare and an electrically insulated thermocouple as well as with a sensitive Schlieren imaging system and with an optical emission spectroscopic method.

2. Methodology

2.1. Cold atmospheric pressure plasma jet

The plasma jet used in this experiment (see figure 1) is a self-designed coaxial dielectric barrier plasma jet inspired by [23, 24]. This CAP-Jet is operated with dry argon as feed gas, operated with a high voltage at a frequency of 22 kHz. It is powered by a flyback power supply (PVM500-1000L, Information Unlimited, US) at up to 3 kV_{pp} operating voltage. Its driven electrode consists of a stainless-steel tube (Ø 2 mm) snugly mounted inside a borosilicate dielectric tube (Ø 4 mm).

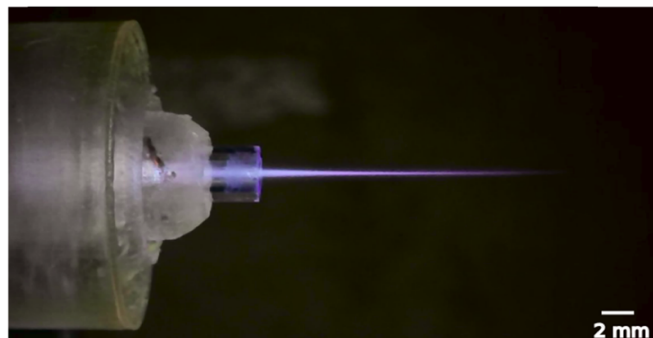


Figure 1. Image of a CAP-Jet plume.

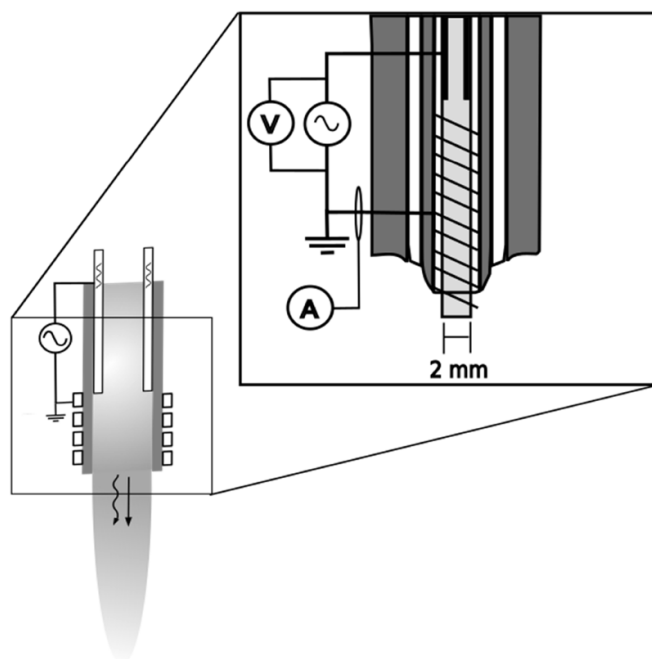


Figure 2. Sketch of a CAP-Jet. The design is based on a coaxial dielectric barrier discharge using a helicoidal grounded electrode.

The grounded electrode consists of a wire which is helically wrapped around the dielectric tube as seen in figure 2. The plasma jet can produce a plume length of up to 2 cm for an argon flow of 2.5 SLM. This agrees well with the findings for non-turbulent plasma flow at higher frequencies [25]. The current and voltage were monitored with a set of voltage probe with a resistor of 2 Ω and a CT4028 voltage probe (Cal Test Electronics, US) respectively.

2.2. FBG

FBG is home-made by periodically structuring an optical fibre using a phase-mask technique as described in detail in [26].

As seen in figure 3, the FBG temperature sensor technique is based on the phenomenon of Bragg wavelength shift, which occurs in response to temperature changes. This wavelength shift is a result of a shift of the thermo-optic coefficient of the optical fibre [27].

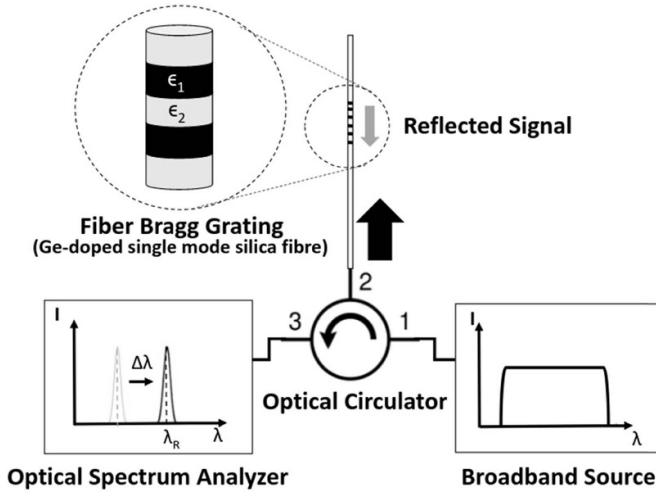


Figure 3. Diagram of FBG temperature measurement setup. A broadband source is sent into a FBG with the use of an optical circulator. When the light reaches the FBG, a sharp, thermally-sensitive signal is reflected and subsequently measured by an optical spectrum analyser.

To actively monitor temperature changes, we integrated a C-band broadband source (BBS, JDS Uniphase, US) into the FBG setup via a fibre-optic circulator. The reflected signal was directed to an ANDO optical spectrum analyser, enabling real time monitoring of Bragg reflection wavelength variations. The FBG sensor's response to temperature is characterized by a shift of 11 pm/K resulting in an uncertainty of 0.1 K.

2.3. Schlieren imaging system

The second method we used to measure the temperature is based on Schlieren imaging. The imaging system is set up in the so-called z-shape configuration [28] (see figure 4). As point light source, a collimated Laser-Diode-Pumped DPSS Laser Module (532 nm, 0.9 mW) is used. In the z-shape setup, the light is collimated from the point source with an aspherical parabolic mirror. A second aspherical parabolic mirror focuses the light onto a razor blade, which acts as a spatial filter in the Fourier plane. The plasma source is installed in the collimated section of the light beam. The system images any variation in the index of refraction. The light is collected by a CMOS camera (Allied Vision Alvium 1800 U-240 m, Edmund Optics, US).

The temperature is derived from an analysis of the relationship between the derivative of the refractive index (n) and the density of the gas, employing the Clausius–Mossotti equation to the first order which is expressed through the Gladstone–Dale relation. This relation comes from the approximation of the Clausius–Mossotti equation in which small variation of index of refraction are assumed. This analysis is performed through the Abel inversion of our signal and can be described by the following expression:

$$\hat{c}(r) = S(n(r) - n_0) = \int_r^\infty \frac{c(y) dy}{\pi \sqrt{y^2 - r^2}}. \quad (1)$$

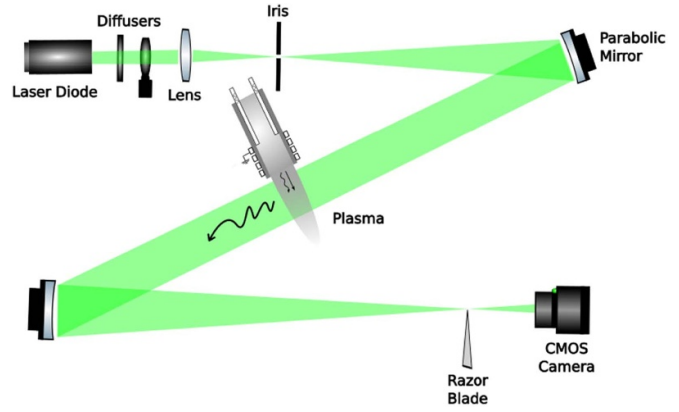


Figure 4. Schlieren measurement setup. The light from a point light source is collimated by a spherical mirror where it is collimated on a second spherical mirror. At the focal point of the second mirror, a razor blade is used to spatially filter the signal before reaching the camera.

Here, S represents the contrast signal within our image. With this expression, we can derive the value of our effective relative refractive index as follows:

$$n_0 + \frac{\hat{c}}{S} - 1 = \frac{N}{N_r} \sum_i \epsilon_{r,i} \chi_i. \quad (2)$$

With the Gladstone–Dale relation that forms a link between the refractive index and the density of the gas ($n-1$) $\propto \rho$, we utilize the following expression to determine the gas temperature based on Schlieren measurements. This approximation is taken directly from the ideal gas law, where $\rho \propto P/T$. The system is calibrated by a measurement of only an argon flow where the room temperature is assumed all throughout the stream. Due to the frequency range the jet is operated in, a laminar flow can be assumed with and without plasma [29]

$$T = T_0 \frac{n_0 + \frac{\hat{c}_{pl.}}{S} - 1}{n_0 + \frac{\hat{c}_{pl.}}{S} - 1} F \quad (3)$$

where F , the factor for change in air mole fractions, is assumed to be nearly equal to 1. Numerically, the Abel inversion was computed using a discretization technique, and each figure was averaged over 200 images. It is important to note that due to the low ionization degree of the plasma source [30], the refractivity of the free electrons could be neglected.

2.4. Thermocouple

The thermocouple measurements were chosen to compare the temperature measurement of the FBG with standard measurement techniques. As a measure to avoid major interference between the instrument and the plasma source, the thermocouple was insulated with a dielectric. A heat shrink tube (polyolefin) was used to cover the probing part of the thermocouple (Type K thermometer, EXTECH Instrument, US). The temperature was manually recorded every 15 s at fixed position controlled via an XYZ positioning system (CNC Genmitsu 3018-PROVer, SainSmart, US) within the accuracy of 100 μm .

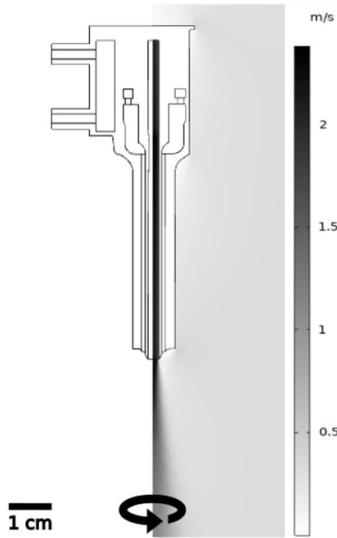


Figure 5. COMSOL simulation of thermal energy dissipation through convection and turbulent diffusion. The velocity of the feed gas is plotted on the right side.

2.5. COMSOL Simulation

The thermal energy dissipation presented in figure 5 was simulated using *COMSOL Multiphysics*. The simulation was generated using the non-isothermal physics module (k - ϵ turbulent flow and heat transfer in fluids). Leveraging the inherent inner rotational symmetry of our plasma source, we configured the model to operate in a two-dimensional space. In this setup, we maintained a steady flow rate of argon at 2.5 SLM and established a constant plasma output temperature of 38 °C. This meticulously controlled simulation was executed to mimic the operation of the plasma source over the duration of 3 min. This extended runtime allowed us to reach a steady-state condition, where the system's parameters and behaviour stabilize, providing a comprehensive understanding of the plasma source's thermal performance over an extended period of time.

2.6. Optical emission spectroscopy

The emission spectrum of the plasma jet was acquired by focussing the emission light of the plasma plume onto a spectrograph (SpectraPro 500i, Acton Research, USA) with a PI Max 2 ICCD camera (Princeton Instrument, USA). With the plume expansion direction parallel to the slit, a 1D spatially dependent measurement of the emission spectrum can be obtained. Each position along the spectrometer slit results in a one-pixel high spectrum. With this setup, two measurements were made: (1) the characterization of the interaction of the plasma with the respective temperature probes and (2) the spatial measurement of the rotational temperature of the plasma jet. To determine the spatially resolved rotational temperature of the jet, the nitrogen emission bands $N_2(C-B)$ were fitted twice using the open source software MassiveOES. As detailed in [31], the software uses a fit of a simulated spectra of

the $N_2(C^3\Pi_u \rightarrow B^3\Pi_g)$ bands. Through a state-by-state fitting procedure, all the quantum states emitting in a specific range are found using a least-square procedure. From the slope of the plotted populations in individual quantum levels divided by their degeneracy and their potential energy, the rotational temperature can be extracted. To enhance the quality of the visualization regarding the fit, data points with uncertainty exceeding the temperature range of interest (35 °C) were removed and a smoothing algorithm was used (Savitzky–Golay filter).

3. Results and discussion

3.1. Effect of the probes on the plasma state

As a way to compare the invasiveness and intrusiveness experienced by introducing a probe into the plume, an emission spectrum using the N_2 emission bands as a reference for rotational temperature variation was used. Figure 6 shows an example of plasma emission and comparison of the different plasma probes. As expected, the bare thermocouple has the biggest impact on the plasma's emission characteristic (and consequently on the plasma conditions). Surprisingly, covering the thermocouple by a dielectric does not dramatically reduce its negative effect on the plasma. Compared to the thermocouple measurements, the FBG probe drastically limits the perturbation of the plasma state. The emission characteristic as shown in figure 6 varies only slightly from the unperturbed plasma effluent, making FBG the least invasive probe technique for temperature measurements. It is also important to note that because of its reduced size, the fibre is much less intrusive in terms of flow.

3.2. Temporal resolution

In figure 7, we present a comparative analysis of the probe's responses to the temporal evolution of the gas temperature using both the FBG technique and the thermocouple. At a distance of 1 cm from the nozzle of the CAP-Jet, the overall temperature of the CAP-Jet saturates near 34 °C. Notably, when the plasma is initially ignited at time $t = 0$ s, two distinct heating phenomena become apparent. The first arises from the plasma's self-heating, leading to a rapid and discernible increase in the recorded temperature. The second phenomenon, associated with the probe's own heat inertia, contributes to the signal in an exponential fashion. The latter effect can be aptly described by Newton's Law of Cooling:

$$T(t) = T_f - (T_f - T_0) \cdot \exp(-t/\tau) \quad (4)$$

where T_f is the terminal temperature, T_0 the initial temperature and τ the response time of the probe. Similarly, once the plasma ceases at $t = 800$ s, the cooling process exhibits a comparable effect. This observation indicates that both temperature probes experience thermal inertia. Although both techniques exhibit a commendable degree of correlation, the thermocouple introduces significantly more uncertainties (± 0.75 K) compared to the FBG (± 0.1 K). It is important to

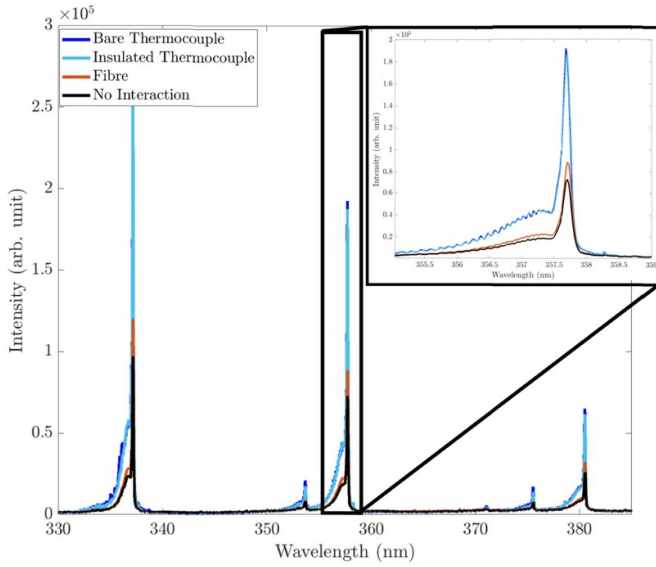


Figure 6. Optical emission spectrum of different interaction mode. The comparison of the relative intensity on nitrogen lines are observed as a way to indicate changes in the plasma state through the rotational temperature. The signal represent the sum of the overall signal of the plume.

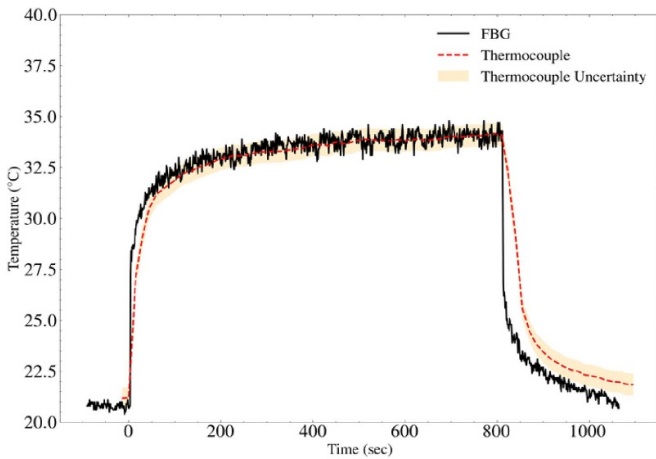


Figure 7. Comparative analysis of the temporal evolution of the gas temperature measured with FBG and a thermocouple.

note that this uncertainty primarily stems from the quality of the instrument.

3.2.1. Characteristic time and effective heat capacity. A fitting procedure on the data shown in figure 7 offers us the means to determine the characteristic time constants inherent to the measurement probes. Remarkably, this procedure unveils a characteristic time of 70.7 s for the FBG and 87.1 s for the thermocouple. These time constants encapsulate the instruments' temporal response to transient temperature variations, reflecting their thermal inertia which can lead us to a calorimetric analysis [32]:

$$\tau = R_e C_e \quad (5)$$

where R_e is the thermal resistance and C_e is the thermal inertia, also expressed by:

$$C_e = m_e c_p \quad (6)$$

where m_e is the mass of the probe and c_p its heat capacity. Similarly, the heat resistance can be obtained through the following equation:

$$R_e = \frac{L}{kA} \quad (7)$$

where L is the length perpendicular to the heat flow, k the heat conductivity and A the cross-section perpendicular to the heat flow. By combining both equations (6) and (7) into equation 5, we can obtain the following expression for the effective heat capacity:

$$c_p = \tau \frac{kA}{Lm_e} \quad (8)$$

For our K-type thermocouple, the thermal resistance can be approximated as a series of interconnected thermal resistors comprised of chromel, alumel, and insulator materials. Leveraging values from [33], we estimate an effective heat capacity of 3.812 J K^{-1} .

With these important parameters, we can undertake a succinct yet comprehensive calorimetric analysis. This methodology, inspired by the pioneering work of [34], enables us to assess the dissipation of heat power within the system. This critical calculation is formulated as:

$$P_{in} = c_p \left(\frac{dT_h}{dt} - \frac{dT_c}{dt} \right) \quad (9)$$

where P_{in} denotes the input heat power, c_p signifies the effective heat capacity, and T_h and T_c represent the temperature signals during both the heating and cooling phases of the thermocouple. Through meticulous analysis and a linear fit applied to the thermocouple's heating and cooling phases, we attain a heat power input value of $1.3 \text{ W} (\pm 0.5 \text{ W})$. Similarly, with a specific heat capacity for the FBG rated at $680 \text{ J Kg}^{-1} \text{ K}^{-1}$, we can estimate the value of $1.2 \text{ W} (\pm 0.6 \text{ W})$, providing a similar value to our power input. The measurement uncertainty yields the error term associated with the covariance of the linear fit. The difference between both values can be explained by the heating of the insulator of the thermocouple that modifies its heat capacity during the measurement [11].

From these values, insights into the efficiency of the plasma source can be used to adapt treatments for better biological response while reducing the heat dissipation.

To assess the significance of our data, the overall power of our source needs to be quantified. By measuring both current and voltage as seen in figure 8, we can get a rough estimate of the power input in the plasma source.

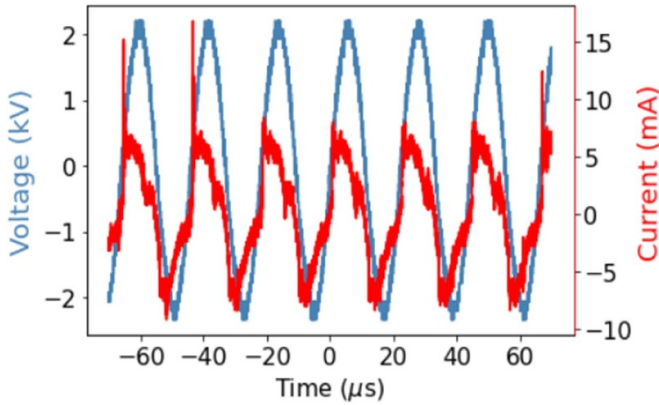


Figure 8. Current and voltage measurements of plasma source.

By using the following relation, we can estimate the power input of our source.

$$P_{\text{average}} = V_{\text{RMS}} I_{\text{RMS}} e^{i\theta} \quad (10)$$

where the root mean square (RMS) of both the voltage V and the current I are multiplied via a scalar product at an angle θ . From figure 8, an angle of 3 degrees is calculated through the analysis of the time step maximizing correlation between both signals. With a duty cycle of 40%, we can estimate our total power to be roughly 2.61 W. This brief power analysis reveals that at least about 50% (both for FBG and thermocouple measurements) of the total power input is dissipated into heat. Due to the approximated nature of the total power measurement, the determined percentage of the power dissipated into heat can only be taken as a minimum estimation.

3.3. Control over the temperature

To control the plasma jet's temperature to be in a bio-compatible range, the energy input is modified by duty cycle control. As shown in figure 9, it becomes considerably easier to monitor the temporal variations in three distinct energy input percentages applied to the plasma jet device. This set of measurements demonstrate the capability to effectively distinguishing between distinct thermal plasma conditions. In comparison to higher energetic conditions, e.g. 50% of duty cycle, the temperature is drastically reduced at a substantially lower energy input scenarios, such as 10% of the total power. Furthermore, our analysis reveals a fairly constant response time of the probe for the different conditions, with an uncertainty of around 4 s. This results express consistency of our probe over multiple conditions. These findings are in line with Newton's law of cooling as the characteristic time is independent of the thermal conditions.

3.4. Spatial thermal correlation of thermocouple, emission spectrum and simulation

In figure 10, an analysis of the plasma gas temperature's spatial distribution is presented.

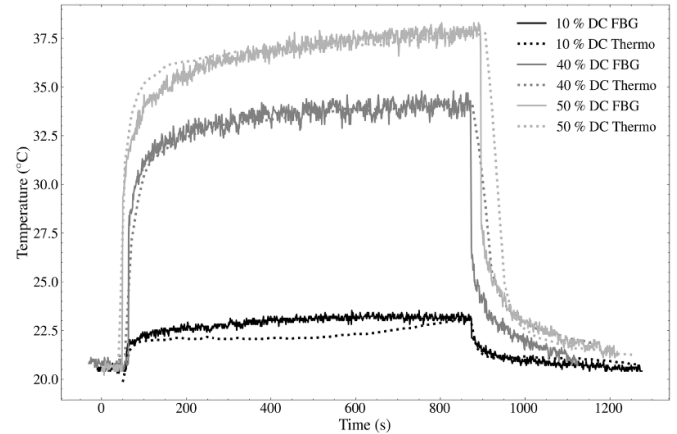


Figure 9. Temporal measurement of plasma jet gas temperature for different energy inputs using the FBG and thermocouple probe. The electric signal input is compared to duty cycle at 10%, 40% and 50%.

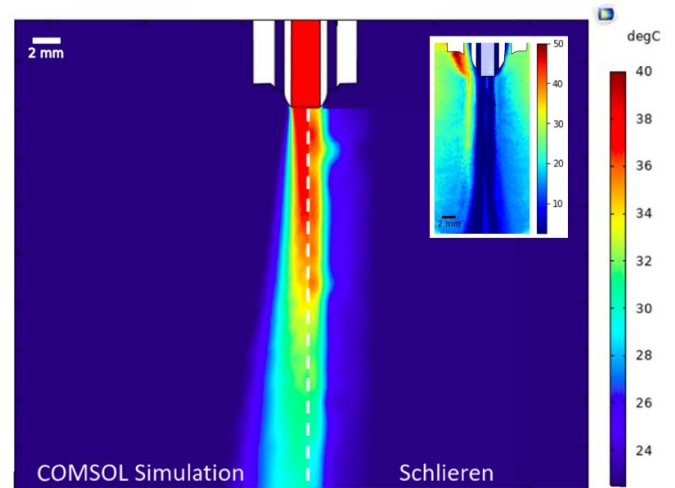


Figure 10. Spatial distribution of a CAP-Jet source with a simulation comparison. A study of the uncertainty is also presented on the top right of the image.

On the right side of the figure, a Schlieren imaging measurement provides 2D information on the gas temperature of the plasma jet, confirming the results obtained via FBG and thermocouple measurements. As expected, the temperature obtained at 1 cm of distance consistently measures $35 \text{ }^\circ\text{C} \pm 5 \text{ }^\circ\text{C}$, reinforcing the reliability and repeatability of our temperature measurements. On the left side of the figure, a COMSOL simulation of a non-isothermal flow has been created as a tool to compare the Schlieren measurements to a simpler case of a heated gas flow for a fixed temperature. A strong correlation between the two sets of results is evident, extending at least 15 mm downstream the nozzle. Beyond this region, a noticeable divergence in the plasma plume's shape can be observed. These regions of divergence correspond with the transition zones between laminar flow and turbulent regime, indicating the influence of flow dynamics on temperature distribution. These findings underscore the

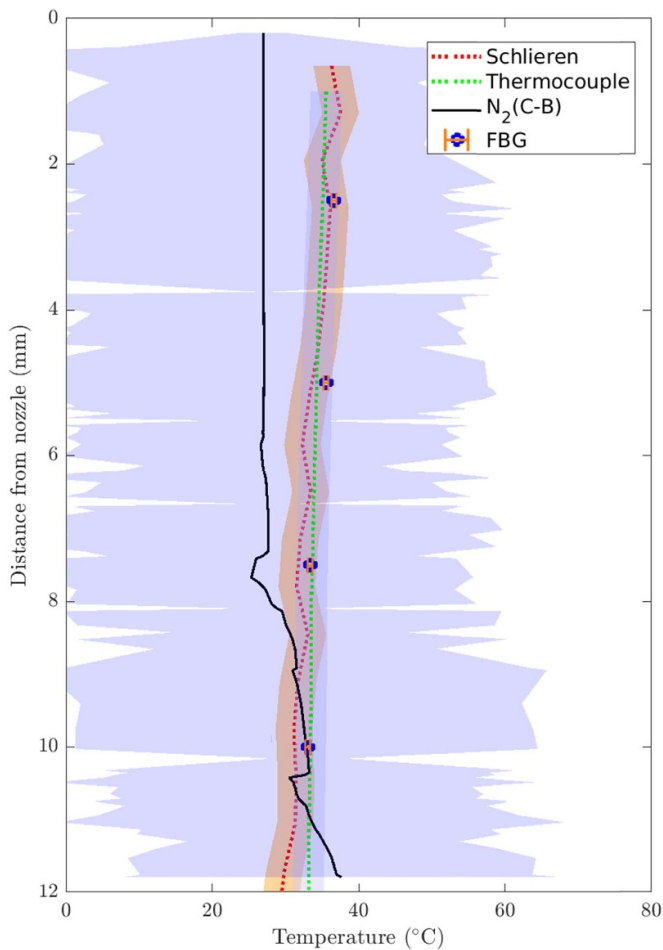


Figure 11. Spatially-resolved thermal distribution of a CAP-Jet source with the schlieren signal, a thermocouple and the rotational temperature from optical emission measurements.

importance of considering flow characteristics when employing Schlieren imaging for temperature measurements, particularly in scenarios where the transitions from laminar to turbulent flow occurs, which introduces substantial deviations in the recorded data.

To compare Schlieren measurements to temperature probe measurements (thermocouple and FBG), the middle vertical section of the Schlieren signal is plotted in comparison to a spatially-resolved measurement of a thermocouple and of a FBG (see figure 11). A clear correlation can be observed. With minimal variation in the order of the uncertainty of the measurements, a similar temperature value and trend can be observed. Additionally, the rotational temperature calculated from a fit of the optical emission spectra of the N_2 C to B emission bands along the plasma plume is plotted. By following the double Boltzmann fitting procedure of the N_2 spectrum as described for argon plasma in [35], the temperature obtained average around $27\text{ °C} \pm 30\text{ °C}$. At first, the temperature range correlate well with what is obtained from other probing methods. However, due to the high uncertainty, this method becomes less relevant for precise knowledge of an argon plasma temperature. For plasma adapted to biological environment with a pure argon inlet, this technique cannot be

used single-handedly to express the global temperature due to its lack of precision.

4. Conclusion

In this work, we used the thermo-optic properties of a FBG as a tool for measuring the gas temperature of a cold plasma jet through direct probing of the effluent. We compared the FBG temperature measurements with thermocouple measurements, Schlieren Imaging measurements and optical emission spectroscopy. For a distance of 1 cm, set as a reference for biological treatments, the temperature measurement techniques show strong correlation at a value of 35 °C . This result confirms the tissue tolerable operating regime of our plasma jet. From the temporal resolution, a simple calorimetric analysis technique was used to provide information on the heat efficiency of the source. Overall, the ability to distinguish and manipulate these thermal trends allow for customization of plasma-based therapy, ultimately expanding the potential application of the technology.

Data availability statement

The data that support the findings of this study are openly available at the following URL/DOI: <https://doi.org/10.5281/zenodo.13671299>.

Acknowledgments

The authors would like to acknowledge the TransMedTech Institute through its main financial partner, the Apogee Canada First Research Excellence Fund. Furthermore, funding through the New Frontiers in Research Funds is gratefully acknowledged. The authors would also like to thank Professor M. R. Wertheimer for providing the spectrograph and ICCD.

Ethical statement

No conflict of interest or violation of ethics code apply.

ORCID iDs

Jean-Baptiste Billeau  <https://orcid.org/0009-0002-3957-061X>

Stephan Reuter  <https://orcid.org/0000-0002-4858-1081>

References

- [1] Bekeschus S, Schmidt A, Weltmann K-D and Von Woedtke T 2016 The plasma jet kINPen—A powerful tool for wound healing *Clin. Plasma Med.* **4** 19–28
- [2] Braný D, Dvorská D, Halašová E and Škovierová H 2020 Cold atmospheric plasma: a powerful tool for modern medicine *Int. J. Mol. Sci.* **21** 2932
- [3] Isbary G et al 2012 Successful and safe use of 2 min cold atmospheric argon plasma in chronic wounds: results of a randomized controlled trial *Br. J. Dermatol.* **167** 404–10

- [4] S. P R, S. K and Y. S 2022 Cold atmospheric plasma-induced oxidative stress and ensuing immunological response—a Neo-Vista in immunotherapy *Free Radic. Res.* **56** 498–510
- [5] Kramer A et al 2008 Polypragmasia in the therapy of infected wounds—conclusions drawn from the perspectives of low temperature plasma technology for plasma wound therapy *GMS Krankenhhyg Interdiszip* vol 3 (available at: www.ncbi.nlm.nih.gov/pmc/articles/PMC2831521/)
- [6] Laroussi M et al 2022 Low-temperature plasma for biology, hygiene, and medicine: perspective and roadmap *IEEE Trans. Radiat. Plasma Med. Sci.* **6** 127–57
- [7] Graves D B 2014 Oxy-nitroso shielding burst model of cold atmospheric plasma therapeutics *Clin. Plasma Med.* **2** 38–49
- [8] Babington P, Rajjoub K, Canady J, Siu A, Keidar M and Sherman J H 2015 Use of cold atmospheric plasma in the treatment of cancer *Biointerphases* **10** 029403
- [9] Stoffels E, Kieft I E and Sladek R E J 2003 Superficial treatment of mammalian cells using plasma needle *J. Phys. D: Appl. Phys.* **36** 2908
- [10] Wertheimer M R, Saoudi B, Ahlawat M and Kashyap R 2012 In situ thermometry in noble gas dielectric barrier discharges at atmospheric pressure *Plasma Process. Polym.* **9** 955–67
- [11] Stahl M, Trottenberg T and Kersten H 2010 A calorimetric probe for plasma diagnostics *Rev. Sci. Instrum.* **81** 023504
- [12] Zaplotnik R, Primc G and Vesel A 2021 Optical emission spectroscopy as a diagnostic tool for characterization of atmospheric plasma jets *Appl. Sci.* **11** 2275
- [13] Moon S Y and Choe W 2003 A comparative study of rotational temperatures using diatomic OH, O₂ and N₂⁺ molecular spectra emitted from atmospheric plasmas *Spectrochim. Acta B* **58** 249–57
- [14] Giuliani L, Gallego J L, Minotti F, Kelly H and Grondona D 2015 Emission spectroscopy of an atmospheric pressure plasma jet operated with air at low frequency *J. Phys.: Conf. Ser.* **591** 012048
- [15] Pietzonka L, Eichhorn C, Scholze F and Spemann D 2023 Laser-induced fluorescence spectroscopy for kinetic temperature measurement of xenon neutrals and ions in the discharge chamber of a radiofrequency ion source *J. Electr. Propuls.* **2** 4
- [16] Luo Y, Lietz A M, Yatom S, Kushner M J and Bruggeman P J 2018 Plasma kinetics in a nanosecond pulsed filamentary discharge sustained in Ar–H₂O and H₂O *J. Phys. D: Appl. Phys.* **52** 044003
- [17] Dilecce G, Martini L M, Tosi P, Scotoni M and Benedictis S D 2015 Laser induced fluorescence in atmospheric pressure discharges *Plasma Sources Sci. Technol.* **24** 034007
- [18] Asghar A H, Ahmed O B and Galaly A R 2021 Inactivation of E. coli using atmospheric pressure plasma jet with dry and wet argon discharges *Membranes* **11** 46
- [19] Schmidt-Bleker A, Reuter S and Weltmann K-D 2015 Quantitative schlieren diagnostics for the determination of ambient species density, gas temperature and calorimetric power of cold atmospheric plasma jets *J. Phys. D: Appl. Phys.* **48** 175202
- [20] Chamorro J C, Prevosto L, Cejas E, Fischfeld G, Kelly H and Mancinelli B 2018 Ambient species density and gas temperature radial profiles derived from a schlieren technique in a low-frequency non-thermal oxygen plasma jet *Plasma Chem. Plasma Process.* **38** 45–61
- [21] Schena E, Tosi D, Saccomandi P, Lewis E and Kim T 2016 Fiber optic sensors for temperature monitoring during thermal treatments: an overview *Sensors* **16** 1144
- [22] Ahlawat M, Saoudi B and Kashyap R 2012 Accurate in-situ gas temperature measurements in dielectric barrier discharges at atmospheric pressure *Appl. Phys. Lett.* **100** 201112
- [23] Es-sebbar E, Bauville G, Fleury M, Pasquiers S and Santos Sousa J 2019 Spatio-temporal distribution of absolute densities of argon metastable 1s5 state in the diffuse area of an atmospheric pressure nanosecond pulsed argon microplasma jet propagating into ambient air *J. Appl. Phys.* **126** 073302
- [24] Douat C, Bauville G, Fleury M, Laroussi M and Puech V 2012 Dynamics of colliding microplasma jets *Plasma Sources Sci. Technol.* **21** 034010
- [25] Darny T, Bauville G, Fleury M, Pasquiers S and Sousa J S 2021 Periodic forced flow in a nanosecond pulsed cold atmospheric pressure argon plasma jet *Plasma Sources Sci. Technol.* **30** 105021
- [26] Kashyap R 2010 Fabrication of bragg gratings *Fiber Bragg Gratings* 2nd edn, ed R Kashyap (Academic) ch 3, pp 53–118
- [27] Kashyap R (ed) 2010 Appendix I *Fiber Bragg Gratings* 2nd edn (Academic) pp 597–9
- [28] Traldi E, Boselli M, Simoncelli E, Stancampiano A, Gherardi M, Colombo V and Settles G S 2018 Schlieren imaging: a powerful tool for atmospheric plasma diagnostic *EPJ Tech. Instrum.* **5** 1–23
- [29] Sousa J S, Niemi K, Cox L J, Algwari Q T, Gans T and O'Connell D 2011 Cold atmospheric pressure plasma jets as sources of singlet delta oxygen for biomedical applications *J. Appl. Phys.* **109** 123302
- [30] Vasil'ev L A 1971 Schlieren methods Jerusalem, Israel Program; [distributed by Keter Inc.] (available at: <http://archive.org/details/schlierenmethods0000vasi>) (Accessed 4 April 2024)
- [31] Voráč J, Kusýn L and Synek P 2019 Deducing rotational quantum-state distributions from overlapping molecular spectra *Rev. Sci. Instrum.* **90** 123102
- [32] Oliveira A V S, Avrit A and Gradeck M 2022 Thermocouple response time estimation and temperature signal correction for an accurate heat flux calculation in inverse heat conduction problems *Int. J. Heat Mass Transfer* **185** 122398
- [33] Park R M, Carrol R M, Burns G W, Desmaris R R, Hall F B, Herkovitz M B, MacKenzie D, McGuire E F, Reed R P and Sparks L L 1993 Manual on the use of thermocouples in temperature measurement, Fourth Edition, Sponsored by ASTM committee E20 on temperature measurement *Micro & Nano Lett.* **290**
- [34] Thornton J A 1978 Substrate heating in cylindrical magnetron sputtering sources *Thin Solid Films* **54** 23–31
- [35] Wang Q, Doll F, Donnelly V M, Economou D J, Sadeghi N and Franz G F 2007 Experimental and theoretical study of the effect of gas flow on gas temperature in an atmospheric pressure microplasma *J. Phys. D: Appl. Phys.* **40** 4202